

# Control of Impurity Phase Segregation in a PdCrO<sub>2</sub>/CuCrO<sub>2</sub> Heterostructure\*

Tom Ichibha<sup>1,†</sup>, Sangmoon Yoon<sup>1,2</sup>, Jong Mok Ok<sup>1,3</sup>, Mina Yoon<sup>1</sup>, Ho Nyung Lee<sup>1</sup>, and Fernando A. Reboredo<sup>1,‡</sup>

<sup>1</sup>*Materials Science and Technology Division, Oak Ridge National Laboratory, Oak Ridge, TN 37831, USA*

<sup>2</sup>*Department of Physics, Gachon University, Seongnam 13306, Republic of Korea and*

<sup>3</sup>*Department of Physics, Pusan National University, Pusan 46241, Republic of Korea*

(Dated: March 16, 2023)

PdCrO<sub>2</sub> films are synthesized on CuCrO<sub>2</sub> buffer layers on Al<sub>2</sub>O<sub>3</sub> substrates. This synthesis is accompanied by impurity phase segregation, which hampers the synthesis of high quality PdCrO<sub>2</sub> films. The potential causes of impurity phase segregation were studied by using a combination of experiments and ab initio calculations. X-ray diffraction and scanning transmission electron microscopy experiments revealed impurity phases of Cu<sub>x</sub>Pd<sub>1-x</sub> alloy and chromium oxides, Cr<sub>2</sub>O<sub>3</sub> and Cr<sub>3</sub>O<sub>4</sub>, in PdCrO<sub>2</sub>. Calculations determined that oxygen deficiency can cause the impurity phase segregation. Therefore, preventing oxygen release from delafossites could suppress the impurity phase segregation. The amounts of Cr<sub>2</sub>O<sub>3</sub> and Cr<sub>3</sub>O<sub>4</sub> depend differently on temperature and oxygen partial pressure. A reasonable theory-based explanation for this experimental observation is provided.

## I. INTRODUCTION

Delafossites are intriguing materials that can combine 2D electronic conductivity in the cation *A* layers and magnetism in slightly distorted octahedra in the *BO*<sub>6</sub> layers, which stack alternately [1–3]. The abundant possible choices of monovalent *A* and trivalent *B* cations lead to a number of delafossite materials with diverse physical properties [4, 5]. The *ABO*<sub>2</sub> delafossites were first reported in 1971 by a group of the DuPont Experimental Station [1–4]. A quarter of century after delafossites were first reported, they received renewed attention when the transparent *p*-type semiconductor CuAlO<sub>2</sub> was discovered [6, 7]. Simultaneously, Tanaka et al.[8] reported the strong anisotropy of electronic conduction for the metallic PdCoO<sub>2</sub> single crystals [3]. One decade later, Takatsu and Maeno et al., working on PdCoO<sub>2</sub> and PdCrO<sub>2</sub>, reported the growth of single crystals of PdCrO<sub>2</sub> [9]. These single crystals exhibit intriguing phenomena[4] such as the unconventional anomalous Hall effect in PdCrO<sub>2</sub>[10] and anomalous temperature dependence of specific heat and electrical resistivity that are driven by high-frequency phonons in PdCoO<sub>2</sub>[10]. Their seminal work originated the continuous study of delafossite metals to this day.

Delafossite metals have electronic conductivity comparable with the most conductive pure metals [3, 4, 8, 11] owing to their remarkably long electronic mean free paths of up to 20 μm [4, 12, 13]. Among delafossite metals, PdCrO<sub>2</sub> is especially interesting because it coexists with a layer-wise non-collinear spin state [14–18] and exhibits high electronic conductivity [16]. Its topological properties, primarily

caused by spin-orbit coupling in Pd, allow for the observation of an unconventional anomalous Hall effect [10, 19] in bulk PdCrO<sub>2</sub>. Additionally, PdCrO<sub>2</sub> films and surfaces have been studied. Angle-resolved photoemission spectroscopy experiments showed that Pd-terminated PdCrO<sub>2</sub> has surface ferromagnetism, which may originate from the Stoner-like instability[20, 21]. Experimental studies of PdCrO<sub>2</sub> films established that the antiferromagnetic spin state remains stable down to a thickness of 3.6 nm [22].

Hybrid layered heterostructures, composed of PdCrO<sub>2</sub> and other delafossite materials, could exhibit interesting and different phenomena than their parent compounds [23]. However, despite the interest in the material, the epitaxial growth of PdCrO<sub>2</sub> films has not been widely studied [22, 24–27]. The growth of PdCrO<sub>2</sub> films on Al<sub>2</sub>O<sub>3</sub> is sometimes accompanied by impurity phases (i.e., Cu<sub>x</sub>Pd<sub>1-x</sub> alloy and chromium oxides) [22]. Recent research discovered that a one-monolayer buffer layer of CuCrO<sub>2</sub> on an Al<sub>2</sub>O<sub>3</sub> substrate suppresses this instability [22]. However, a nonnegligible amount of impurity phase is still formed. Understanding the mechanism of the impurity phase segregation and how to suppress it is highly desired for the growth of heterostructures containing PdCrO<sub>2</sub> or other Pd-based delafossites.

In this work, the mechanism of impurity phase segregation of a heterostructure of a PdCrO<sub>2</sub> layer with a CuCrO<sub>2</sub> buffer layer on an Al<sub>2</sub>O<sub>3</sub> substrate was studied using a combination of experiments and ab initio calculations. X-ray diffraction (XRD) and scanning transmission electron microscopy (STEM) experiments were performed, and the segregation of Cu<sub>x</sub>Pd<sub>1-x</sub> alloy and chromium oxide (Cr<sub>2</sub>O<sub>3</sub> and Cr<sub>3</sub>O<sub>4</sub>) impurity phases was observed. These experiments revealed that the formation of Cr<sub>2</sub>O<sub>3</sub> negatively correlates with oxygen partial pressure, whereas the formation of Cr<sub>3</sub>O<sub>4</sub> does not correlate with oxygen partial pressure. Moreover, the Cr<sub>2</sub>O<sub>3</sub> (Cr<sub>3</sub>O<sub>4</sub>) formation weakly (strongly) positively correlates with temperature. The segregation of Cu<sub>x</sub>Pd<sub>1-x</sub> alloy and chromium oxide impurity phases must be accompanied by the appearance or disappearance of point defects because the segregation processes are not stoichiometric. In this scenario, calculations revealed that oxygen vacancies can cause the impurity phase segregation. Calculations also revealed that the

\* This manuscript has been authored by UT-Battelle, LLC, under contract DE-AC05-00OR22725 with the US Department of Energy (DOE). The US government retains and the publisher, by accepting the article for publication, acknowledges that the US government retains a nonexclusive, paid-up, irrevocable, worldwide license to publish or reproduce the published form of this manuscript, or allow others to do so, for US government purposes. DOE will provide public access to these results of federally sponsored research in accordance with the DOE Public Access Plan (<http://energy.gov/downloads/doe-public-access-plan>).

<sup>†</sup> ichibha@icloud.com

<sup>‡</sup> reboredofa@ornl.gov

segregation of  $\text{Cr}_2\text{O}_3$  or  $\text{Cr}_3\text{O}_4$  is energetically the most favorable among the chromium oxides, agreeing with the experiments described in Section III A. Finally, the calculations also revealed that the formation of  $\text{Cr}_2\text{O}_3$  and  $\text{Cr}_3\text{O}_4$  depends on temperature and oxygen partial pressure.

## II. EXPERIMENTAL AND CALCULATION DETAILS

### A. Experimental details

A  $\text{PdCrO}_2$  layer with thickness of approximately 10 nm was grown on a one-monolayer ( $\sim 0.38$  nm)  $\text{CuCrO}_2$  buffer layer on an  $\text{Al}_2\text{O}_3$  substrate via pulsed laser deposition using polycrystalline targets. Before the film growth, commercially available  $\text{Al}_2\text{O}_3$  (0001) substrates (CrysTec, Germany) were annealed at  $1100^\circ\text{C}$  for 1 h to achieve atomically flat surfaces with step-terrace structure. For  $\text{PdCrO}_2$  films, the growth conditions were widely varied: temperature ( $T$ ) was  $500\text{--}800^\circ\text{C}$ , and oxygen partial pressure ( $P_{\text{O}_2}$ ) was  $10\text{--}500$  mTorr. The repetition rate and fluence of KrF excimer laser ( $\lambda = 248$  nm) were fixed at 5 Hz and  $1.5\text{ J/cm}^2$ , respectively. The cross-sectional STEM specimens were prepared using low-energy ion milling at  $\text{LN}_2$  temperature after mechanical polishing. High-angle annular dark field (HAADF) STEM measurements were performed on a Nion UltraSTEM200 operated at 200 kV. The microscope is equipped with a cold-field emission gun and a third- and fifth-order aberration corrector for sub-angstrom resolution. The convergence half-angle of 30 mrad was used, and the inner angle of the HAADF STEM was approximately 65 mrad.

### B. Calculation details

Density functional theory (DFT) implemented in the VASP package [28] was used to understand the energetics of competing phases during the experimental growth process. The Perdew–Burke–Ernzerhof (PBE)+ $U$  method [29, 30] was used. The Hubbard  $U$  correction was applied to the  $3d$  shell of the Cr atoms. The  $U$  value was 3.3 eV, which was optimized compared with the results of the HSE06 functional [31], as described in the Supporting Information. The core electrons were replaced with pseudopotentials made by the projector-augmented wave method accompanied by the VASP code [32–34]. The cutoff energy was 520 eV, and  $k$ -spacing was  $0.30\text{ \AA}^{-1}$ , which converged the Cr vacancy formation energy in  $\text{CuCrO}_2$  within 2 meV. Experimental lattice vectors for  $\text{CuCrO}_2$  [35],  $\text{PdCrO}_2$  [36], and  $\text{Al}_2\text{O}_3$  were used [37]. The lattice vectors reported in the Materials project [38] were used for chromium oxides and chromium metal [39]. The atomic coordinates were relaxed for the functional. The convergence criteria for the self-consistent field and ionic cycles were  $1.0 \times 10^{-7}$  eV and  $1.0 \times 10^{-6}$  eV, respectively.

## III. RESULTS AND DISCUSSIONS

### A. Segregation of impurity phases

Impurity phases including  $\text{Cu}_x\text{Pd}_{1-x}$ ,  $\text{Cr}_2\text{O}_3$ , and  $\text{Cr}_3\text{O}_4$  have been observed experimentally [40]. In Figure 1 we show in addition to  $2\theta$ - $\theta$  XRD spectrum, the intensity of the XRD data as a function of the growth conditions. As reported in Ref. [22], the high-quality  $\text{PdCrO}_2$  films can be achieved only within a relatively narrow growth window. Outside the growth window, the metallic properties are severely deteriorated by the impurity formation. The resistance could not be measured because of the high resistivity. The rectangular boxes in Figure 1 highlight the main impurities observed in XRD:  $\text{Cr}_3\text{O}_4$  and  $\text{Cr}_2\text{O}_3$ . The bottom two panels of Figure 1 map the XRD intensities of  $\text{Cr}_3\text{O}_4$  and  $\text{Cr}_2\text{O}_3$  for temperature and oxygen partial pressure. The relative abundances between  $\text{Cr}_3\text{O}_4$  and  $\text{Cr}_2\text{O}_3$  are difficult to assess quantitatively using the XRD intensities because the XRD reflectivity varies with substances and angles. However, we use the intensities to assess qualitatively how the formation of each substance is affected by growth conditions. The XRD intensity of  $\text{Cr}_3\text{O}_4$  strongly positively correlates with temperature (correlation coefficient [41]  $\rho = +0.82$ ), whereas the correlation between the XRD intensity of  $\text{Cr}_2\text{O}_3$  and temperature is weak ( $\rho = +0.19$ ). Moreover,  $\text{Cr}_3\text{O}_4$ 's peak strength does not depend on oxygen partial pressure ( $\rho = +0.01$ ), but  $\text{Cr}_2\text{O}_3$ 's peak strength negatively depends on oxygen partial pressure ( $\rho = -0.48$ ). These results are compared with our calculations in the last paragraph of Section III F.

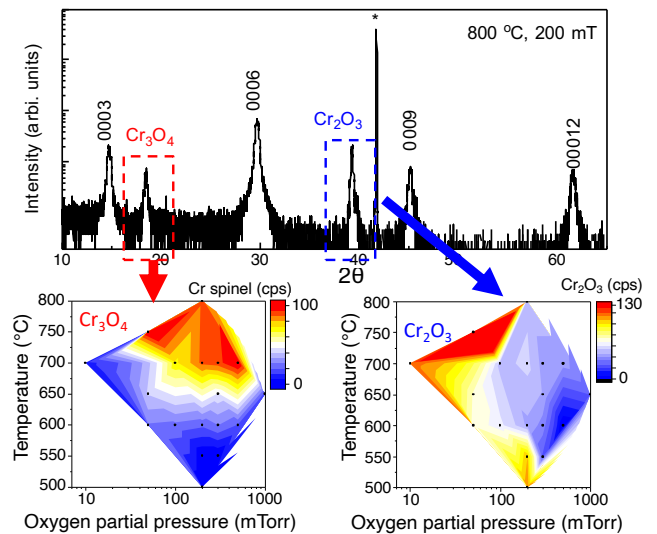


FIG. 1. XRD spectrum and mapping of XRD peak strengths of  $\text{Cr}_3\text{O}_4$  and  $\text{Cr}_2\text{O}_3$  for temperature and oxygen partial pressure. This measurement was performed for an approximately 6 nm  $\text{PdCrO}_2$  film grown on a one-monolayer  $\text{CuCrO}_2$  buffer layer.

## B. Point-defect formation energy

Because the system segregates oxygen-deficient oxides  $\text{Cr}_2\text{O}_3$  or  $\text{Cr}_3\text{O}_4$ , the segregation process should be accompanied by the appearance or disappearance of point defects. The ratio of O to Cr (O/Cr) in  $\text{Cr}_2\text{O}_3$  is  $\text{O/Cr} = 1.5$ . In  $\text{Cr}_3\text{O}_4$ , O/Cr is about 1.3. In the delafossite materials, O/Cr is 2.0. Therefore, the formation energies of multiple types of point self-defects in bulk  $\text{Al}_2\text{O}_3$ ,  $\text{CuCrO}_2$ , and  $\text{PdCrO}_2$  were calculated. To simplify the problem, defects in the bulk were calculated, even though samples with different thickness of  $\text{PdCrO}_2$  and  $\text{CuCrO}_2$  films have been grown in this and other works [22, 40].

The following describes the notation used for the point defects and explains how to evaluate the formation energies.  $V_{\text{Cr}}$ ,  $V_{\text{Cu}}$ ,  $V_{\text{Pd}}$ , and  $V_{\text{O}}$  indicate vacancies in the Cr, Cu, Pd, and O sites. The Cu (Pd) replacement defects in the Cr sites, or *antisite defects*, are indicated by  $\text{Cu}_{\text{Cr}}$  ( $\text{Pd}_{\text{Cr}}$ ). Larger defect complexes such as  $\text{Cu}_{\text{Cr}}\&V_{\text{Cu}}$  ( $\text{Pd}_{\text{Cr}}\&V_{\text{Pd}}$ ) can form when Cu (Pd) atoms move to a preformed  $V_{\text{Cr}}$ , leaving the  $V_{\text{Cr(Pd)}}$ . The formation energies of these defects are given as follows: for  $\text{CuCrO}_2$ ,

$$\Delta E(V_{\alpha}) = E(\text{CuCrO}_2)_{V_{\alpha}} - E(\text{CuCrO}_2)_{\text{bulk}} + \mu_{\alpha}, \quad (\alpha = \text{Cu, Cr, or O}), \quad (1)$$

$$\Delta E(\text{Cu}_{\text{Cr}}\&V_{\text{Cu}}) = E(\text{CuCrO}_2)_{\text{Cu}_{\text{Cr}}\&V_{\text{Cu}}} - E(\text{CuCrO}_2)_{\text{bulk}} + \mu_{\text{Cr}}, \quad (2)$$

and for  $\text{PdCrO}_2$ ,

$$\Delta E(V_{\alpha}) = E(\text{PdCrO}_2)_{V_{\alpha}} - E(\text{PdCrO}_2)_{\text{bulk}} + \mu_{\alpha}, \quad (\alpha = \text{Pd, Cr or O}), \quad (3)$$

$$\Delta E(\text{Pd}_{\text{Cr}}\&V_{\text{Pd}}) = E(\text{PdCrO}_2)_{\text{Pd}_{\text{Cr}}\&V_{\text{Pd}}} - E(\text{PdCrO}_2)_{\text{bulk}} + \mu_{\text{Cr}}. \quad (4)$$

Here,  $E(\text{CuCrO}_2)_{\text{bulk}}$  and  $E(\text{PdCrO}_2)_{\text{bulk}}$  are the total energies of pristine delafossite structures.  $E(\text{CuCrO}_2)_X$  and  $E(\text{PdCrO}_2)_X$  are the total energies of structures with type- $X$  defects. The chemical potential of atomic species  $\alpha$  is  $\mu_{\alpha}$ . The oxygen vacancy formation energy in the  $\text{Al}_2\text{O}_3$  substrate was also calculated by

$$\Delta E(V_{\text{O}}) = E(\text{Al}_2\text{O}_3)_{V_{\text{O}}} - E(\text{Al}_2\text{O}_3)_{\text{bulk}} + \mu_{\text{O}}. \quad (5)$$

Our experiments observed the Cu-Pd alloy and Cr oxide impurity phases on the composite sample of  $\text{Al}_2\text{O}_3$ ,  $\text{CuCrO}_2$ , and  $\text{PdCrO}_2$  (see § III A). The defect formation energies should be evaluated for the experimental conditions: the chemical equilibrium states consisting of  $\text{Al}_2\text{O}_3$ ,  $\text{CuCrO}_2$ ,  $\text{PdCrO}_2$ ,  $\text{Cu}_x\text{Pd}_{1-x}$ , and a chromium oxide. The exact value of  $x$  in  $\text{Cu}_x\text{Pd}_{1-x}$  is not known experimentally. The ratio  $x$  potentially depends on the volume comparison of  $\text{CuCrO}_2$  and  $\text{PdCrO}_2$ . However, the change in the results is negligible when  $x$  changes from 0.5 to 0.25 or 0.75 (variations of only 0.33 eV were observed), as described in the Supporting Information. Therefore, the results reported below assumed  $x = 0.5$ . Solving the following equations yields the chemical potentials. For

example, if  $\text{Al}_2\text{O}_3$ ,  $\text{CuCrO}_2$ ,  $\text{PdCrO}_2$ ,  $\text{CuPd}$ , and  $\text{Cr}_3\text{O}_4$  coexist, then

$$2\mu_{\text{Al}} + 3\mu_{\text{O}} = E(\text{Al}_2\text{O}_3), \quad (6)$$

$$\mu_{\text{Cu}} + \mu_{\text{Cr}} + 2\mu_{\text{O}} = E(\text{CuCrO}_2), \quad (7)$$

$$\mu_{\text{Pd}} + \mu_{\text{Cr}} + 2\mu_{\text{O}} = E(\text{PdCrO}_2), \quad (8)$$

$$\mu_{\text{Cu}} + \mu_{\text{Pd}} = E(\text{CuPd}), \quad (9)$$

$$3\mu_{\text{Cr}} + 4\mu_{\text{O}} = E(\text{Cr}_3\text{O}_4). \quad (10)$$

There exist as many independent linear equations as unknown chemical potentials, so the chemical potentials are trivially determined.

## C. Formation energies of defects as a function of the chemical potentials

The formation energies of point defects in  $\text{Al}_2\text{O}_3$ ,  $\text{CuCrO}_2$ , and  $\text{PdCrO}_2$  were calculated for different chromium oxides, as described in Section III B. We also considered the Cr metal as the Cr source of the Cr-rich limit. The results are summarized in Figure 2. The point-defect formation energies are all positive, so  $\text{CuCrO}_2$  and  $\text{PdCrO}_2$  are thermodynamically stable and stoichiometric under the considered chemical conditions. For low values of the oxygen chemical potential ( $\lesssim -8.6$  eV), the  $V_{\text{O}}$  in  $\text{CuCrO}_2$  and  $\text{PdCrO}_2$  have the lowest formation energies; the  $V_{\text{O}}$  in  $\text{Al}_2\text{O}_3$  is much higher. As soon as the oxygen chemical potential increases, the  $V_{\text{Cu}}$  and  $V_{\text{Pd}}$  become the lowest formation energy defects. The Cr vacancies, by contrast, have much higher formation energies. The experimental chemical potentials are not well defined because the system is out of equilibrium, as described in Section III B. However, each element's stability corresponds to anywhere between the vertical lines that correspond to the oxygen chemical potentials with  $\text{Cr}_3\text{O}_4$  and  $\text{Cr}_2\text{O}_3$ . The  $V_{\text{Cr}}$ ,  $\text{Cu}_{\text{Cr}}\&V_{\text{Cu}}$ , and  $\text{Pd}_{\text{Cr}}\&V_{\text{Pd}}$  are all Cr-deficient point defects. For  $\text{CuCrO}_2$ , the formation energy of  $\text{Cu}_{\text{Cr}}\&V_{\text{Cu}}$  is lower than that of  $V_{\text{Cr}}$ . Therefore, the Cr site does not have a vacancy because a neighboring Cu occupies the Cr site by forming  $V_{\text{Cu}}$  next to  $\text{Cu}_{\text{Cr}}$ .

## D. Instability of $\text{CuCrO}_2$ and $\text{PdCrO}_2$ for oxygen-deficient samples

Experiments found the segregation of impurity phases of  $\text{Cu}_x\text{Pd}_{1-x}$ ,  $\text{Cr}_2\text{O}_3$ , and  $\text{Cr}_3\text{O}_4$  on a 10 nm  $\text{PdCrO}_2$  layer with a one-monolayer  $\text{CuCrO}_2$  buffer layer on an  $\text{Al}_2\text{O}_3$  substrate. The samples were grown under low oxygen partial pressures. The simultaneous presence of seven compounds ( $\text{CuCrO}_2$ ,  $\text{PdCrO}_2$ ,  $\text{Cu}_x\text{Pd}_{1-x}$ ,  $\text{Cr}_2\text{O}_3$ ,  $\text{Cr}_3\text{O}_4$ ,  $\text{O}_2$ , and  $\text{Al}_2\text{O}_3$ ) but only five chemical elements complicates the theoretical analysis. Finding a solution for the chemical potential equations is impossible when the equations outnumber the independent variables. In this case, the system is out of equilibrium. The chemical potentials may not be uniform throughout the sample. For instance, near the surface, the oxygen chemical potential may be a function of temperature and oxygen

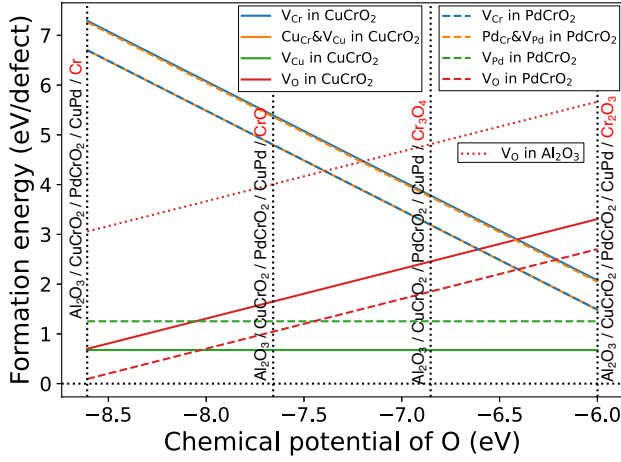


FIG. 2. Formation energies of intrinsic point defects in  $\text{CuCrO}_2$ ,  $\text{PdCrO}_2$ , and  $\text{Al}_2\text{O}_3$  calculated by the PBE+ $U$  method as a function of the oxygen chemical potential. The chemical potentials are calculated for  $\text{CuCrO}_2$ ,  $\text{PdCrO}_2$ ,  $\text{Al}_2\text{O}_3$ ,  $\text{CuPd}$ , and different chromium oxides.

partial pressure. By contrast, near the regions where  $\text{Cr}_2\text{O}_3$  and  $\text{Cr}_3\text{O}_4$  coexist, the chemical potentials of Cr and O are uniquely determined by the formation energies of the two solids. Alternatively, near the  $\text{Al}_2\text{O}_3$  substrate, the oxygen chemical potential may be determined by temperature and the concentration of oxygen vacancies in  $\text{Al}_2\text{O}_3$ .

The impurity phases are oxygen deficient (i.e., chromium rich) relative to  $\text{CuCrO}_2$  and  $\text{PdCrO}_2$ : the O/Cr ratios of  $\text{Cr}_2\text{O}_3$  (1.5) and  $\text{Cr}_3\text{O}_4$  (~1.3) are smaller than that of  $\text{CuCrO}_2$  and  $\text{PdCrO}_2$  (2.0). To elucidate the possible cause of impurity phase segregation, several different possible reactions originating from out-of-equilibrium states were considered. Then their potential to destabilize  $\text{CuCrO}_2$  and  $\text{PdCrO}_2$  was examined. The analysis revealed that low oxygen partial pressures and high temperatures could explain the segregation of  $\text{Cr}_2\text{O}_3$  and  $\text{Cu}_x\text{Pd}_{1-x}$ . Preexisting defects as energetic as oxygen vacancies in  $\text{Al}_2\text{O}_3$  could enhance the segregation of  $\text{Cr}_3\text{O}_4$  and  $\text{Cu}_x\text{Pd}_{1-x}$ .

### E. Thermochemical reactions

To simplify the analysis, the  $\text{Cu}_x\text{Pd}_{1-x}$  alloy is assumed to be  $\text{CuPd}$ , as described in the last paragraph of Section III B. The theoretical approach shows that the combination of  $\text{CuCrO}_2$  and  $\text{PdCrO}_2$  is stable against the  $\text{CrO}_2$  and  $\text{CuPd}$  impurity phase segregation, which is a stoichiometric process. The thermochemical equation of this segregation is

$$E(\text{CuCrO}_2) + E(\text{PdCrO}_2) = E(\text{CuPd}) + 2E(\text{CrO}_2) + Q(\text{CrO}_2), \quad (11)$$

where  $Q(\text{CrO}_2)$  is the energy gained, or lost if negative, to form  $\text{CrO}_2$ . The value of  $Q(\text{CrO}_2)$  was calculated to be

-1.102 eV per two formula units of  $\text{CrO}_2$ , so this reaction is endothermic.

By contrast, the Cr/O ratios of  $\text{CuCrO}_2$  and  $\text{PdCrO}_2$  vs.  $\text{Cr}_2\text{O}_3$  or  $\text{Cr}_3\text{O}_4$  are different. Therefore, the impurity phase segregation may be caused by an impurity-absorbing defect. For  $\text{Cr}_2\text{O}_3 + \text{CuPd}$ , the impurity phase segregation may be caused and promoted by an oxygen-adsorbent mechanism because the Cr/O ratios of  $\text{CuCrO}_2$  and  $\text{PdCrO}_2$  (1/2) and  $\text{Cr}_2\text{O}_3$  (2/3) are different. This oxygen deficiency may be the result of low environmental oxygen concentration relative to chromium from either (i) defective  $\text{CuCrO}_2$ ,  $\text{PdCrO}_2$ , or  $\text{Al}_2\text{O}_3$  or (ii) low oxygen content in the vacuum growth chamber [42]. For mechanism (i), preexisting  $\text{V}_\text{O}$  in  $\text{CuCrO}_2$ ,  $\text{PdCrO}_2$ , or  $\text{Al}_2\text{O}_3$  and formation of Cr-deficient defects such as  $\text{V}_\text{Cr}$  in  $\text{CuCrO}_2$  or  $\text{PdCrO}_2$  were considered to keep the Cr/O ratios constant before and after the process [43].

Therefore, the energy gain obtained by the (dis)appearance of point defects in  $\text{CuCrO}_2$ ,  $\text{PdCrO}_2$ , and  $\text{Al}_2\text{O}_3$  was compared with the release of oxygen molecules into the oxygen gas in the growth chamber. All these possibilities were considered as particle exchanges with a particle bath.

The energy cost of taking an atom ( $\alpha = \text{O}$  or  $\text{Cr}$ ) from one of these particle baths is defined as

$$\nu_\alpha \equiv E(\text{bath})_{\text{bulk}} - E(\text{bath})_\alpha. \quad (12)$$

Here,  $E(\text{bath})_{\text{bulk}}$  and  $E(\text{bath})_\alpha$  are the energies of the particle bath without defects and with an  $\alpha = \text{O}$  or  $\text{Cr}$  vacancy, respectively [44].

The thermochemical equations for the segregation of  $\text{Cr}_2\text{O}_3$  when introducing O to or removing Cr from the particle bath are given as follows:

$$E(\text{CuCrO}_2) + E(\text{PdCrO}_2) = E(\text{CuPd}) + E(\text{Cr}_2\text{O}_3) + \nu_\text{O} + Q(\text{Cr}_2\text{O}_3, \text{V}_\text{O}^{\text{rem}}), \quad (13)$$

$$E(\text{CuCrO}_2) + E(\text{PdCrO}_2) = E(\text{CuPd}) + (4/3)E(\text{Cr}_2\text{O}_3) - (2/3)\nu_\text{Cr} + Q(\text{Cr}_2\text{O}_3, \text{V}_\text{Cr}^{\text{int}}). \quad (14)$$

In equation (13), the term  $\nu_\text{O}$  takes into account the effect of removing an oxygen vacancy in the particle bath, and  $-(2/3)\nu_\text{Cr}$  considers the effect of creating a fraction of Cr vacancies in the particle bath.

Similarly, the segregation of  $\text{Cr}_3\text{O}_4$  could be explained by the following reactions:

$$E(\text{CuCrO}_2) + E(\text{PdCrO}_2) = E(\text{CuPd}) + (2/3)E(\text{Cr}_3\text{O}_4) + (4/3)\nu_\text{O} + Q(\text{Cr}_3\text{O}_4, \text{V}_\text{O}^{\text{rem}}), \quad (15)$$

$$E(\text{CuCrO}_2) + E(\text{PdCrO}_2) = E(\text{CuPd}) + E(\text{Cr}_3\text{O}_4) - \nu_\text{Cr} + Q(\text{Cr}_3\text{O}_4, \text{V}_\text{Cr}^{\text{int}}). \quad (16)$$

Their derivations are described in detail in Appendix A.

The exothermic energies,  $Q$ , are shown in eqs (13)–(16), for different values of  $\nu_\text{O}$  and  $\nu_\text{Cr}$ , depending on the particle baths

in Table I. The table shows that only  $Q(\text{Cr}_2\text{O}_3, V_{\text{O}}^{\text{rem}})$  and  $Q(\text{Cr}_3\text{O}_4, V_{\text{O}}^{\text{rem}})$  can be positive (i.e., exothermic reaction), whereas the reactions involving the formation of Cr-deficient defects are always endothermic. Therefore, the preexisting oxygen vacancies could explain the spontaneous segregation of  $\text{Cr}_2\text{O}_3$ ,  $\text{Cr}_3\text{O}_4$ , and CuPd impurity phases.

Figure 3 shows  $Q(\text{Cr}_2\text{O}_3, V_{\text{O}}^{\text{rem}})$  and  $Q(\text{Cr}_3\text{O}_4, V_{\text{O}}^{\text{rem}})$  in Table I for different  $\nu_{\text{O}}$  (i.e., different particle bath). The stability of oxygen atoms in each particle bath negatively correlates with  $\nu_{\text{O}}$ : oxygen atoms are the most (least) stable in  $\text{Al}_2\text{O}_3$  ( $\text{O}_2$  gas).  $Q(\text{Cr}_2\text{O}_3, V_{\text{O}}^{\text{rem}})$  changes depending on  $-\nu_{\text{O}}$ , as given in eq (13). Similarly,  $Q(\text{Cr}_3\text{O}_4, V_{\text{O}}^{\text{rem}})$  changes depending on  $-(4/3)\nu_{\text{O}}$ , as given in eq (15). The impurity phase segregation is endothermic when  $\text{O}_2$  gas is the particle bath and exothermic for the other particle baths. The energetically favored chromium oxide changes from  $\text{Cr}_2\text{O}_3$  to  $\text{Cr}_3\text{O}_4$  with  $\nu_{\text{O}}$  decreasing from PdCrO<sub>2</sub> to  $\text{Al}_2\text{O}_3$ .

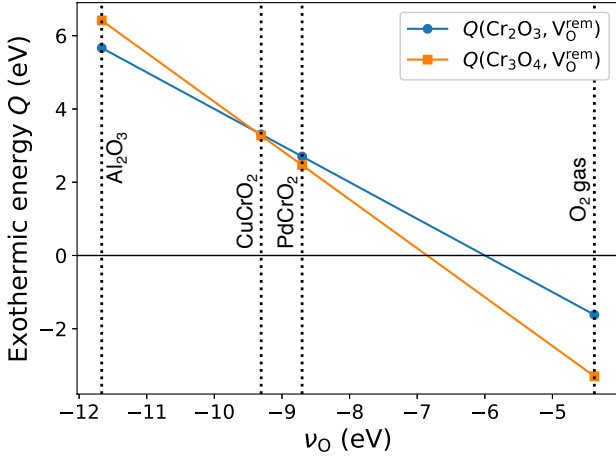


FIG. 3. Plots of  $Q(\text{Cr}_2\text{O}_3, V_{\text{O}}^{\text{rem}})$  and  $Q(\text{Cr}_3\text{O}_4, V_{\text{O}}^{\text{rem}})$  shown in Table I for different  $\nu_{\text{O}}$  (i.e., different O particle baths).

#### F. Entropy contributions to the formation of $\text{Cr}_2\text{O}_3$ and $\text{Cr}_3\text{O}_4$

In this section, entropy contributions to the positive  $Q(\text{Cr}_2\text{O}_3, V_{\text{O}}^{\text{rem}})$  and  $Q(\text{Cr}_3\text{O}_4, V_{\text{O}}^{\text{rem}})$  are considered. For convenience,  $Q(\text{Cr}_2\text{O}_3) \equiv Q(\text{Cr}_2\text{O}_3, V_{\text{O}}^{\text{rem}})$  and  $Q(\text{Cr}_3\text{O}_4) \equiv Q(\text{Cr}_3\text{O}_4, V_{\text{O}}^{\text{rem}})$ .

Entropy contributions depend on the temperature, point-defect densities, and oxygen partial pressure. The energies  $E$  were replaced by Helmholtz free energies  $F(T)$  in eqs (13) and (15). For bulk structures,  $F(T)$  was evaluated by

$$F(T) = E + F_{\text{vib}}(T). \quad (17)$$

Here,  $F_{\text{vib}}(T)$  is the vibrational free energy. For  $\nu_{\text{O}}$  in a defective solid, the vacancy configurational entropy contribution

was considered in addition to  $F_{\text{vib}}(T)$ . If the vacancy density is  $c_{\text{v}}$ , then the free energy change when removing one vacancy is

$$\Delta F_{\text{config}}(T, c_{\text{v}}) = k_{\text{B}}T[-\ln(c_{\text{v}}) + \ln(1 - c_{\text{v}})] \quad (18)$$

(details in Appendix B). Here,  $k_{\text{B}}$  is the Boltzmann constant. Therefore,  $Q(\text{Cr}_2\text{O}_3)$  and  $Q(\text{Cr}_3\text{O}_4)$  depend on vacancy density and temperature when the bath location is a defective solid.

When considering the case of  $\text{O}_2$  released into the growth chamber, because the experimental oxygen partial pressure is very low and the temperature is high, the translational entropy contribution could significantly stabilize the oxygen gas. This stabilization may change  $Q(\text{Cr}_2\text{O}_3)$  and  $Q(\text{Cr}_3\text{O}_4)$  from negative to positive. Without entropy contributions, they are negative, as shown in Table I. The Helmholtz free energy  $F(T)$  of the oxygen gas per molecule is defined as

$$F(T, P_{\text{O}_2}) = E(\text{O}_2) + F_{\text{vib}}(T) + F_{\text{rot}}(T) + F_{\text{trans}}(T, P_{\text{O}_2}) \quad (19)$$

Here,  $E(\text{O}_2)$  is the energy of an isolated oxygen molecule and  $F_{\text{vib}}(T)$ ,  $F_{\text{rot}}(T)$ , and  $F_{\text{trans}}(T, P_{\text{O}_2})$  are free energies by vibrational, rotational, and translational entropies, respectively. Then  $F_{\text{rot}}(T)$  and  $F_{\text{trans}}(T, P_{\text{O}_2})$  [45] are given by

$$F_{\text{rot}}(T) = -k_{\text{B}}T \left( 1 + \ln \frac{8\pi^2 I k_{\text{B}}T}{2h^2} \right), \quad (20)$$

$$F_{\text{trans}}(T, P_{\text{O}_2}) = -k_{\text{B}}T \ln \frac{k_{\text{B}}T}{P_{\text{O}_2} \Lambda^3}, \quad (21)$$

$$\Lambda \equiv \frac{h}{\sqrt{2\pi m k_{\text{B}}T}} \quad (22)$$

Here,  $h$  is the Planck constant, and  $I$  is the moment of inertia of an oxygen molecule. Therefore,  $Q(\text{Cr}_2\text{O}_3)$  and  $Q(\text{Cr}_3\text{O}_4)$  depend on oxygen partial pressure and temperature when the bath location is the dilute oxygen gas.

The entropy contributions in eqs (13) and (15) yield  $Q(\text{Cr}_2\text{O}_3)$  and  $Q(\text{Cr}_3\text{O}_4)$  for different bath locations and conditions. In these equations, the bulk free energies depend on only the temperature. When the bath is a defected crystal,  $\nu_{\text{O}}$  depends on temperature and vacancy density. When the bath is the oxygen gas,  $\nu_{\text{O}}$  depends on temperature and oxygen partial pressure. When  $\nu_{\text{O}}$ 's entropy contributions are ignored,  $Q(\text{Cr}_2\text{O}_3)$  and  $Q(\text{Cr}_3\text{O}_4)$  barely depend on the temperature:  $Q(\text{Cr}_2\text{O}_3)$  and  $Q(\text{Cr}_3\text{O}_4)$  do not change more than 60 meV from 600 to 1000 K, and  $Q(\text{Cr}_2\text{O}_3) - Q(\text{Cr}_3\text{O}_4)$  does not change more than 11 meV from 600 to 1000 K. Therefore, the dependence of  $Q(\text{Cr}_2\text{O}_3)$  and  $Q(\text{Cr}_3\text{O}_4)$  on the conditions is almost equivalent to that of  $\nu_{\text{O}}$ .

To understand the conditions under which different oxides might be generated experimentally, different baths for exchanging oxygen were systematically considered. When the bath is a defected crystal,  $\nu_{\text{O}}$  was calculated for vacancy densities in the range of  $10^{-8}$ – $10^{-1}$  per site and temperatures in the range of 600–1000 K. When the bath is the oxygen gas,  $\nu_{\text{O}}$  was calculated for oxygen partial pressures in the range of  $10^{-6}$ – $10^0$  atm and temperatures in the range of 600–1000 K.

TABLE I. Exothermic energies,  $Q$  in eqs (13)–(16), for the formation of  $\text{Cr}_2\text{O}_3$  or  $\text{Cr}_3\text{O}_4$  and  $\text{CuPd}$  accompanied by  $V_{\text{O}}^{\text{rem}}$ 's removal from or  $V_{\text{Cr}}^{\text{int}}$ 's introduction to different bath locations.

Bath location	$Q(\text{Cr}_2\text{O}_3, V_{\text{O}}^{\text{rem}})$	$Q(\text{Cr}_2\text{O}_3, V_{\text{Cr}}^{\text{int}})$	$Q(\text{Cr}_3\text{O}_4, V_{\text{O}}^{\text{rem}})$	$Q(\text{Cr}_3\text{O}_4, V_{\text{Cr}}^{\text{int}})$
PdCrO <sub>2</sub>	<b>+2.703</b>	-0.990	<b>+2.466</b>	-3.192
CuCrO <sub>2</sub>	<b>+3.308</b>	-0.989	<b>+3.273</b>	-3.189
Al <sub>2</sub> O <sub>3</sub>	<b>+5.666</b>	–	<b>+6.417</b>	–
O <sub>2</sub> in vacuum ( $T = 0$ )	-1.619	–	-3.297	–

Figure 4 shows a map of the  $\nu_{\text{O}}$  calculated for different bath locations. The vertical width of each area indicates the variation width corresponding to vacancy densities in the range of  $10^{-8}$ – $10^{-1}$  per site or oxygen partial pressures in the range of  $10^{-6}$ – $10^0$  atm. Figure 4 is divided into the three regions I–III according to the corresponding  $Q(\text{Cr}_2\text{O}_3)$  and  $Q(\text{Cr}_3\text{O}_4)$  values. The region I is  $Q(\text{Cr}_2\text{O}_3, \text{Cr}_3\text{O}_4) < 0$ : the impurity phase segregation does not proceed spontaneously. The region II is  $Q(\text{Cr}_2\text{O}_3) > 0$  and  $Q(\text{Cr}_2\text{O}_3) > Q(\text{Cr}_3\text{O}_4)$ :  $\text{Cr}_2\text{O}_3 + \text{Cu}_x\text{Pd}_{1-x}$  is spontaneously predominantly formed. The region III is  $Q(\text{Cr}_3\text{O}_4) > Q(\text{Cr}_2\text{O}_3) > 0$ :  $\text{Cr}_3\text{O}_4 + \text{Cu}_x\text{Pd}_{1-x}$  is spontaneously predominantly formed. Therefore, when the particle bath is oxygen gas, CuCrO<sub>2</sub>, or PdCrO<sub>2</sub>, the majority of chromium oxide is  $\text{Cr}_2\text{O}_3$ . When the particle bath is Al<sub>2</sub>O<sub>3</sub>, the majority of chromium oxide is  $\text{Cr}_3\text{O}_4$ .

Furthermore, other bath locations than the above listed are realistically possible. For example, an oxygen-terminated PdCrO<sub>2</sub> surface could lead to very high  $\nu_{\text{O}}$ . By contrast, a Pd-terminated surface could lead to very low  $\nu_{\text{O}}$ . Investigation of such further complicated mechanisms is a possible future work for theory and experiments.

These calculations revealed that  $\nu_{\text{O}}$  in O<sub>2</sub> gas decreases with decreasing oxygen partial pressure, and  $\nu_{\text{O}}$  in defected crystals decreases with increasing  $c_{\text{v}}$  (details in supporting information). This result is not surprising because it indicates that gaseous oxygen molecules are more stable under oxygen-poor conditions. In reality,  $c_{\text{v}}$  would negatively correlate with oxygen partial pressure, so  $\nu_{\text{O}}$  positively correlates with oxygen partial pressure in every bath location: lower oxygen partial pressure facilitates the segregation of impurity phases. This analysis agrees with the experimental finding described in Section III A:  $\text{Cr}_2\text{O}_3$  formation negatively correlates with oxygen partial pressure.

However, this analysis does not explain the independence of  $\text{Cr}_3\text{O}_4$  formation on oxygen partial pressure. Rather,  $\text{Cr}_3\text{O}_4$  formation strongly depends on temperature, unlike  $\text{Cr}_2\text{O}_3$ . Some hypotheses are considered to explain the  $\text{Cr}_3\text{O}_4$  experimental results. (i) Most of the bath locations belong to region II in Figure 4, and the temperature determines how much the metastable  $\text{Cr}_3\text{O}_4$  is segregated. (ii) Some of the bath locations belong to region III, but high barrier energy is required to transfer oxygen atoms, moving oxygen vacancies, so the temperature determines the oxygen exchange rate.

For example, the barrier energy required to transfer oxygen atoms from Al<sub>2</sub>O<sub>3</sub> to the surface would be higher than from PdCrO<sub>2</sub> to the surface. To verify the hypotheses, sad-

dle state analyses by methods such as the nudged elastic band method, molecular dynamics, and/or modeling the sample's surface should be applied in future works.

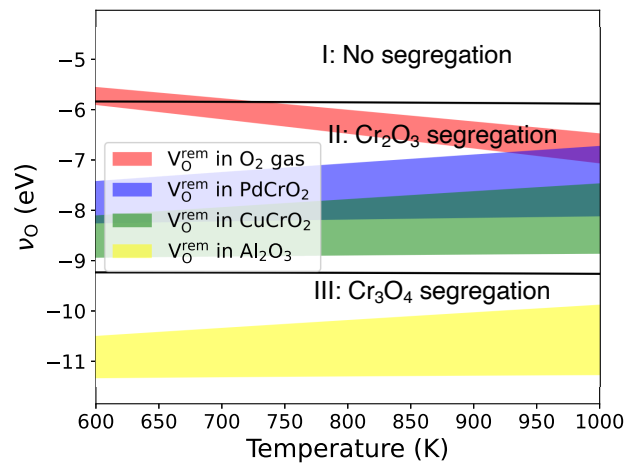


FIG. 4. Plots of the energy of the oxygen sink ( $\nu_{\text{O}}$ ) using eq (12) for different possible locations in the experimental range of temperatures and estimated concentration. The upper and lower edges of  $V_{\text{O}}^{\text{rem}}$  in O<sub>2</sub> gas are  $P_{\text{O}_2} = 1$  and  $10^{-6}$  atm. The upper and lower edges of the other areas are  $c_{\text{v}} = 10^{-1}$  and  $10^{-8}$  per site. The dark green area between the blue and green areas is the overlap of the blue and green areas.

#### IV. CONCLUSION

The mechanism of impurity phase segregation with the epitaxial growth of a PdCrO<sub>2</sub> layer on a CuCrO<sub>2</sub> buffer layer on an Al<sub>2</sub>O<sub>3</sub> substrate was investigated via a combination of experiments and ab initio calculations. XRD experiments revealed the formation of  $\text{Cu}_x\text{Pd}_{1-x}$  alloy and chromium oxide ( $\text{Cr}_2\text{O}_3$  and  $\text{Cr}_3\text{O}_4$ ) impurity phases. Consequently, the impurity phase segregation should be involved with appearance or disappearance of point defects or oxygen migration because the possible segregation processes are not stoichiometric. In this scenario, several possible mechanisms of impurity phase segregation were considered with oxygen vacancy disappearance or chromium vacancy appearance into different particle baths: Al<sub>2</sub>O<sub>3</sub>, CuCrO<sub>2</sub>, PdCrO<sub>2</sub>, and the dilute oxygen gas. Calculations established that the oxygen vacancy consumption processes are energetically favorable and supported ex-

perimental evidence that  $\text{Cr}_2\text{O}_3$  or  $\text{Cr}_3\text{O}_4$  are the predominant chromium oxide impurity phases. Specifically, preventing the release of oxygen atoms from delafossite materials could suppress the impurity phase segregation.

## APPENDIX

### A. Derivation of eqs (13) and (14)

For ease of explanation, let the particle bath be  $\text{PdCrO}_2$ . Consider the following thermochemical equations for the segregation of  $\text{Cr}_2\text{O}_3$  by removing preexisting O vacancies or creating Cr vacancies.

$$\begin{aligned} & E(\text{CuCrO}_2)_{\text{bulk}}^{(n)} + E(\text{PdCrO}_2)_{\text{V}_\text{O}}^{(n)} \\ &= E(\text{CuCrO}_2)_{\text{bulk}}^{(n-1)} + E(\text{PdCrO}_2)_{\text{bulk}}^{(n-1)} \\ &+ E(\text{CuPd}) + E(\text{Cr}_2\text{O}_3) + Q(\text{Cr}_2\text{O}_3, \text{V}_\text{O}^{\text{rem}}) \end{aligned} \quad (23)$$

and

$$\begin{aligned} & E(\text{CuCrO}_2)_{\text{bulk}}^{(n)} + E(\text{PdCrO}_2)_{\text{bulk}}^{(n)} \\ &= E(\text{CuCrO}_2)_{\text{bulk}}^{(n-1)} + E(\text{PdCrO}_2)_{(2/3)\text{V}_\text{Cr}}^{(n-1)} \\ &+ E(\text{CuPd}) + (4/3)E(\text{Cr}_2\text{O}_3) + Q(\text{Cr}_2\text{O}_3, \text{V}_\text{Cr}^{\text{int}}). \end{aligned} \quad (24)$$

Here, for example,  $E(\text{CuCrO}_2)_{\text{bulk}}^{(n)}$  is the energy of  $n$  f.u. bulk  $\text{CuCrO}_2$ ,  $E(\text{PdCrO}_2)_{\text{V}_\text{O}}^{(n)}$  is the energy of  $n$  f.u.  $\text{PdCrO}_2$  with an oxygen vacancy,  $E(\text{PdCrO}_2)_{(2/3)\text{V}_\text{Cr}}^{(n-1)}$  is the energy of  $(n-1)$  f.u.  $\text{PdCrO}_2$  with a fraction of  $2/3$  chromium vacancies, and  $E(\text{CuPd})$  is the energy of 1 f.u. bulk  $\text{CuPd}$ . For the bulk, the following relationships hold according to the definitions.

$$E(\text{CuCrO}_2)_{\text{bulk}}^{(n)} = n E(\text{CuCrO}_2), \quad (25)$$

$$E(\text{PdCrO}_2)_{\text{bulk}}^{(n)} = n E(\text{PdCrO}_2). \quad (26)$$

Define the energy gain from removing  $m$  oxygen or chromium vacancies in  $n\text{PdCrO}_2$  as follows:

$$\nu_\text{O}(n, m) \equiv E(\text{PdCrO}_2)_{\text{bulk}}^{(n)} - E(\text{PdCrO}_2)_{m\text{V}_\text{O}}^{(n)}, \quad (27)$$

$$\nu_\text{Cr}(n, m) \equiv E(\text{PdCrO}_2)_{\text{bulk}}^{(n)} - E(\text{PdCrO}_2)_{m\text{V}_\text{Cr}}^{(n)}. \quad (28)$$

In the thermodynamic limit ( $n \rightarrow \infty$ ), the following relationships should hold:

$$\nu_{\text{O,Cr}}(n, m) \simeq \nu_{\text{O,Cr}}(n-1, m), \quad (29)$$

$$\nu_{\text{O,Cr}}(n, m) \simeq m \nu_{\text{O,Cr}}(n, 1), \quad (30)$$

Moreover, define

$$\nu_{\text{O,Cr}} \equiv \nu_{\text{O,Cr}}(n, 1) \quad (31)$$

These are the  $\nu_\alpha$  defined in eq (12). Applying eqs (25)–(31) to eqs (23) and (24), yields eqs (13) and (14).

### B. Configurational entropy of removing a vacancy.

When  $n$  vacancies exist in  $N$  sites, the configurational entropy is

$$S(N, n) = k_B \ln \frac{N!}{(N-n)!n!}. \quad (32)$$

The entropy change achieved by adding one vacancy is given by

$$\begin{aligned} \Delta S(N, n) &\equiv S(N, n+1) - S(N, n) \\ &= k_B [-\ln(c_v + 1/N) + \ln(1 - c_v)], \end{aligned} \quad (33)$$

$$c_v \equiv n/N. \quad (34)$$

For the limit of  $N \rightarrow \infty$  with fixed  $c_v$ ,

$$\Delta S(N, n) \rightarrow \Delta S(c_v) = k_B [-\ln(c_v) + \ln(1 - c_v)] \quad (35)$$

Therefore, the free energy change achieved by removing one vacancy is given by

$$\Delta F(T, c_v) = -T(-S(c_v)) \quad (36)$$

$$= k_B T [-\ln(c_v) + \ln(1 - c_v)]. \quad (37)$$

## V. ACKNOWLEDGMENTS

We acknowledge E. Heinrich for valuable help with manuscript preparation. This work was supported by the US Department of Energy, Office of Science, Basic Energy Sciences, Materials Sciences and Engineering Division (theory and synthesis) and as part of the Computational Materials Sciences Program and Center for Predictive Simulation of Functional Materials (structural characterization). VESTA [46] was used to draw the crystal structures.

- 
- [1] R. D. Shannon, D. B. Rogers, and C. T. Prewitt, Chemistry of noble metal oxides. I. Syntheses and properties of  $\text{ABO}_2$  delafossite compounds, *Inorganic Chemistry* **10**, 713 (1971), <https://doi.org/10.1021/ic50098a011>.
- [2] R. D. Shannon, C. T. Prewitt, and D. B. Rogers, Chemistry of noble metal oxides. II. Crystal structures of platinum cobalt dioxide, palladium cobalt dioxide, copper iron dioxide,

and silver iron dioxide, *Inorganic Chemistry* **10**, 719 (1971), <https://doi.org/10.1021/ic50098a012>.

- [3] R. D. Shannon, D. B. Rogers, C. T. Prewitt, and J. L. Gillson, Chemistry of noble metal oxides. III. Electrical transport properties and crystal chemistry of  $\text{ABO}_2$  compounds with the delafossite structure, *Inorganic Chemistry* **10**, 723 (1971), <https://doi.org/10.1021/ic50098a013>.

- [4] A. P. Mackenzie, The properties of ultrapure delafossite metals, *Reports on Progress in Physics* **80**, 032501 (2017).
- [5] H. N. Abdelhamid, Delafossite nanoparticle as new functional materials: Advances in energy, nanomedicine and environmental applications, *Materials Science Forum* **832**, 28 (2015).
- [6] H. Kawazoe, M. Yasukawa, H. Hyodo, M. Kurita, H. Yanagi, and H. Hosono, *P*-type electrical conduction in transparent thin films of  $\text{CuAlO}_2$ , *Nature* **389**, 939 (1997).
- [7] H. Yanagi, S. ichiro Inoue, K. Ueda, H. Kawazoe, H. Hosono, and N. Hamada, Electronic structure and optoelectronic properties of transparent *p*-type conducting  $\text{CuAlO}_2$ , *Journal of Applied Physics* **88**, 4159 (2000).
- [8] M. Tanaka, M. Hasegawa, and H. Takei, Growth and Anisotropic Physical Properties of  $\text{PdCoO}_2$  Single Crystals, *Journal of the Physical Society of Japan* **65**, 3973 (1996), <https://doi.org/10.1143/JPSJ.65.3973>.
- [9] H. Takatsu and Y. Maeno, Single crystal growth of the metallic triangular-lattice antiferromagnet  $\text{PdCrO}_2$ , *Journal of Crystal Growth* **312**, 3461 (2010).
- [10] H. Takatsu, S. Yonezawa, S. Fujimoto, and Y. Maeno, Unconventional Anomalous Hall Effect in the Metallic Triangular-Lattice Magnet  $\text{PdCrO}_2$ , *Phys. Rev. Lett.* **105**, 137201 (2010).
- [11] M. Tanaka, M. Hasegawa, and H. Takei, Crystal growth of  $\text{PdCoO}_2$ ,  $\text{PtCoO}_2$  and their solid-solution with delafossite structure, *Journal of Crystal Growth* **173**, 440 (1997).
- [12] C. W. Hicks, A. S. Gibbs, A. P. Mackenzie, H. Takatsu, Y. Maeno, and E. A. Yelland, Quantum oscillations and high carrier mobility in the delafossite  $\text{PdCoO}_2$ , *Phys. Rev. Lett.* **109**, 116401 (2012).
- [13] P. Kushwaha, V. Sunko, P. J. W. Moll, L. Bawden, J. M. Riley, N. Nandi, H. Rosner, M. P. Schmidt, F. Arnold, E. Hassinger, T. K. Kim, M. Hoesch, A. P. Mackenzie, and P. D. C. King, Nearly free electrons in a *5d* delafossite oxide metal, *Science Advances* **1**, 10.1126/sciadv.1500692 (2015).
- [14] J.-P. Doumerc, A. Wichainchai, A. Ammar, M. Pouchard, and P. Hagenmuller, On magnetic properties of some oxides with delafossite-type structure, *Materials Research Bulletin* **21**, 745 (1986).
- [15] M. Mekata, T. Sugino, A. Oohara, Y. Oohara, and H. Yoshizawa, Magnetic structure of antiferromagnetic  $\text{PdCrO}_2$  possible degenerate helices on a rhombohedral lattice, *Physica B: Condensed Matter* **213-214**, 221 (1995).
- [16] H. Takatsu, H. Yoshizawa, S. Yonezawa, and Y. Maeno, Critical behavior of the metallic triangular-lattice heisenberg antiferromagnet  $\text{PdCrO}_2$ , *Phys. Rev. B* **79**, 104424 (2009).
- [17] H. Takatsu, G. Néner, H. Kadowaki, H. Yoshizawa, M. Enderle, S. Yonezawa, Y. Maeno, J. Kim, N. Tsuji, M. Takata, Y. Zhao, M. Green, and C. Broholm, Magnetic structure of the conductive triangular-lattice antiferromagnet  $\text{PdCrO}_2$ , *Phys. Rev. B* **89**, 104408 (2014).
- [18] D. Billington, D. Ernsting, T. E. Millichamp, C. Lester, S. B. Dugdale, D. Kersh, J. A. Duffy, S. R. Giblin, J. W. Taylor, P. Manuel, D. D. Khalyavin, and H. Takatsu, Magnetic frustration, short-range correlations and the role of the paramagnetic fermi surface of  $\text{PdCrO}_2$ , *Scientific Reports* **5**, 10.1038/srep12428 (2015).
- [19] J. M. Ok, Y. J. Jo, K. Kim, T. Shishidou, E. S. Choi, H.-J. Noh, T. Oguchi, B. I. Min, and J. S. Kim, Quantum oscillations of the metallic triangular-lattice antiferromagnet  $\text{PdCrO}_2$ , *Phys. Rev. Lett.* **111**, 176405 (2013).
- [20] F. Mazzola, V. Sunko, S. Khim, H. Rosner, P. Kushwaha, O. J. Clark, L. Bawden, I. Marković, T. K. Kim, M. Hoesch, A. P. Mackenzie, and P. D. C. King, Itinerant ferromagnetism of the Pd-terminated polar surface of  $\text{PdCoO}_2$ , *Proc. Natl. Acad. Sci. U.S.A.* **115**, 12956 (2018).
- [21] T. Harada, Thin-film growth and application prospects of metallic delafossites, *Materials Today Advances* **11**, 100146 (2021).
- [22] J. M. Ok, M. Brahlek, W. S. Choi, K. M. Roccapiore, M. F. Chisholm, S. Kim, C. Sohn, E. Skoropata, S. Yoon, J. S. Kim, and H. N. Lee, Pulsed-laser epitaxy of metallic delafossite  $\text{PdCrO}_2$  films, *APL Mater.* **8**, 051104 (2020).
- [23] F. Lechermann and R. Richter, Theoretical design of highly correlated electron states in delafossite heterostructures, *Phys. Rev. Research* **2**, 013352 (2020).
- [24] T. Harada, K. Fujiwara, and A. Tsukazaki, Highly conductive  $\text{PdCoO}_2$  ultrathin films for transparent electrodes, *APL Materials* **6**, 046107 (2018).
- [25] J. Sun, M. R. Barone, C. S. Chang, M. E. Holtz, H. Paik, J. Schubert, D. A. Muller, and D. G. Schlom, Growth of  $\text{PdCoO}_2$  by ozone-assisted molecular-beam epitaxy, *APL Materials* **7**, 121112 (2019).
- [26] M. Brahlek, G. Rimal, J. M. Ok, D. Mukherjee, A. R. Mazza, Q. Lu, H. N. Lee, T. Z. Ward, R. R. Unocic, G. Eres, and S. Oh, Growth of metallic delafossite  $\text{PdCoO}_2$  by molecular beam epitaxy, *Phys. Rev. Materials* **3**, 093401 (2019).
- [27] P. Yordanov, W. Sigle, P. Kaya, M. E. Gruner, R. Pentcheva, B. Keimer, and H.-U. Habermeier, Large thermopower anisotropy in  $\text{PdCoO}_2$  thin films, *Phys. Rev. Materials* **3**, 085403 (2019).
- [28] G. Kresse and J. Furthmüller, Efficient iterative schemes for ab initio total-energy calculations using a plane-wave basis set, *Phys. Rev. B* **54**, 11169 (1996).
- [29] J. P. Perdew, K. Burke, and M. Ernzerhof, Generalized Gradient Approximation Made Simple, *Phys. Rev. Lett.* **77**, 3865 (1996).
- [30] S. L. Dudarev, G. A. Botton, S. Y. Savrasov, C. J. Humphreys, and A. P. Sutton, Electron-energy-loss spectra and the structural stability of nickel oxide: An LSDA+U study, *Phys. Rev. B* **57**, 1505 (1998).
- [31] J. Heyd, G. E. Scuseria, and M. Ernzerhof, Hybrid functionals based on a screened coulomb potential, *The Journal of Chemical Physics* **118**, 8207 (2003), <https://doi.org/10.1063/1.1564060>.
- [32] P. E. Blöchl, Projector augmented-wave method, *Phys. Rev. B* **50**, 17953 (1994).
- [33] G. Kresse and D. Joubert, From ultrasoft pseudopotentials to the projector augmented-wave method, *Phys. Rev. B* **59**, 1758 (1999).
- [34] D. Hobbs, G. Kresse, and J. Hafner, Fully unconstrained noncollinear magnetism within the projector augmented-wave method, *Phys. Rev. B* **62**, 11556 (2000).
- [35] M. Frontzek, J. T. Haraldsen, A. Podlesnyak, M. Matsuda, A. D. Christianson, R. S. Fishman, A. S. Sefat, Y. Qiu, J. R. D. Copley, S. Barilo, S. V. Shiryayev, and G. Ehlers, Magnetic excitations in the geometric frustrated multiferroic  $\text{CuCrO}_2$ , *Phys. Rev. B* **84**, 094448 (2011).
- [36] M. D. Le, S. Jeon, A. I. Kolesnikov, D. J. Voneshen, A. S. Gibbs, J. S. Kim, J. Jeong, H.-J. Noh, C. Park, J. Yu, T. G. Perring, and J.-G. Park, Magnetic interactions in  $\text{PdCrO}_2$  and their effects on its magnetic structure, *Phys. Rev. B* **98**, 024429 (2018).
- [37] The room temperature structure of Ref. [47] was used.
- [38] A. Jain, S. P. Ong, G. Hautier, W. Chen, W. D. Richards, S. Dacek, S. Cholia, D. Gunter, D. Skinner, G. Ceder, and K. a. Persson, The Materials Project: A materials genome approach to accelerating materials innovation, *APL Materials* **1**, 011002 (2013).
- [39] The database ID for each material: Cr = mp-90, CrO = mp-19091,  $\text{Cr}_3\text{O}_4$  = mp-756253, and  $\text{Cr}_2\text{O}_3$  = mp-19399.



- [40] S. Yoon, J. M. Ok, T. Ichiba, S.-H. Kang, A. Huon, M. Yoon, P. Ganesh, F. A. Reboledo, H. Miao, A. R. Lupini, and H. N. Lee, Templated epitaxy of PdCrO<sub>2</sub> delafossites using atomic sacrificial layers (Unpublished).
- [41] The correlation coefficient  $r$  indicates the strength of correlation between two data-series,  $\{X_i\}_{i=1}^n$  and  $\{Y_i\}_{i=1}^n$ .  $r$  can be from -1 to +1.  $r = +1$  (-1) indicates the complete positive (negative) correlation between  $\{X_i\}_{i=1}^n$  and  $\{Y_i\}_{i=1}^n$ . The correlation coefficient is defined by
- $$r = \frac{\sigma_{X,Y}}{\sigma_X \sigma_Y}. \quad (38)$$
- Here,  $\sigma_X$  and  $\sigma_Y$  are the standard deviations of  $\{X_i\}_{i=1}^n$  and  $\{Y_i\}_{i=1}^n$ .  $\sigma_{X,Y}$  is the covariance of the two data-series:
- $$\sigma_{XY} = \frac{1}{n} \sum_{i=1}^n (X_i - \bar{X})(Y_i - \bar{Y}). \quad (39)$$
- [42] The samples were grown under < 1000 mTorr oxygen partial pressure.
- [43] Preexisting point defects with extra Cr, such as Cr<sub>Pd</sub> and Cr<sub>Cu</sub>, were not considered because their existence explains the appearance of Cr<sub>x</sub>O<sub>1-x</sub> but not Cu<sub>y</sub>Pd<sub>1-y</sub> without involving multiple types defects to balance the chemical reaction.
- [44]  $\nu_\alpha$  is conceptually similar to the chemical potential of  $\alpha$ , but chemical potentials are not defined for a nonequilibrium process.
- [45] D. L. Goodstein, States of matter (Dover Publications, Inc., 1985) pp. 98–105.
- [46] K. Momma and F. Izumi, *VESTA3* for three-dimensional visualization of crystal, volumetric and morphology data, *Journal of Applied Crystallography* **44**, 1272 (2011).
- [47] S. Kondo, K. Tateishi, and N. Ishizawa, Structural evolution of corundum at high temperatures, *Japanese Journal of Applied Physics* **47**, 616 (2008).